Supporting information

Mn-Tuned Active Microenvironment for Synergistic Regulation of Key Intermediate Adsorption in High-Performance Alkaline Water Splitting

Hao Yi[a, b], Wenyu Yan[a, b], Fei Qi[a, b], Zhongke Luo[a, b], Menghan Li[a], Chao Wang[a,b*]

[a] *Institute of Advanced Energy Material and Systems, College of Materials Science and Engineering, North University of China, Taiyuan, 030051 China.*

[b] *Shanxi Key Laboratory of Efficient Hydrogen Storage & Production Technology and Application, Taiyuan, 030051 China.*

[*] Corresponding author: Tel. / Fax: 18634419920. E-mail: wangchao_nuc@126.com

1.1. Material characterization

The crystal structure of the material was investigated using an X-ray diffractometer (XRD, BX'Pert PRO MPD). Testing was conducted in continuous scan mode with a Cu-target Kα radiation source at an operating voltage of 45 kV and a current of 40 mA. The scan range was 5°-90° (2θ) at a scan rate of 5°/min.

The sample morphology was examined using a scanning electron microscope (SEM, Hitachi Regulus 8100) in secondary electron mode. Transmission electron microscopy (TEM) was performed using a JEOL JEM 2100F instrument at an acceleration voltage of 200 kV in bright-field (BF) imaging mode, combined with simultaneous microarea compositional analysis using an EDAX energy dispersive X-ray spectrometer.

X-ray photoelectron spectroscopy (XPS) measurements were performed on a ThermoFisher ESCALAB 250Xi spectrometer in the United States. An Al Kα radiation source (hv = 1486.6 eV) was employed, with an analysis chamber vacuum of 8×10^{-10} Pa. Charge compensation was performed using C 1s = 284.80 eV as the reference energy.

In-situ Raman spectroscopy was performed using a Horiba LabRAM HR Evolution spectrometer with an excitation laser wavelength of 532 nm. The test voltage ranged from 1.1 V to 1.6 V vs. RHE.

1.2. Experimental section

1.2.1. Chemicals and reagents

Ni-foam (NF) with 1mm thickness produced by Kunshan Baiyida, Nickel nitrate hexahydrate (Ni(NO3)2·6H2O,), cobalt nitrate hexahydrate (Co(NO3)2·6H2O, 98%), iron nitrate nonahydrate (Fe(NO3)3·9H2O,99%), zinc nitrate hexahydrate (Zn(NO3)2·6H2O), manganese nitrate tetrahydrate (Mn(NO3)2·4H2O,98%), 2-methylimidazole (C4H6N2, 98%), sodium hypophosphite monohydrate (NaPO2H2·H2O, 99%), potassium hydroxide (KOH 95%), methanol and deionized water are used as they are without further purification.

1.2.2. Synthesis of NCFZM/NF

Before the experiment, foam nickel (NF) with a size of 2 × 3 cm and a thickness of 1 mm was placed in 3M HCl, anhydrous ethanol and deionized water for ultrasonic cleaning for 15 minutes, and then dried in a vacuum oven at 60 ℃ for 6 hours. Dissolve nickel nitrate hexahydrate (0.5 mmol), cobalt nitrate hexahydrate (0.5 mmol), iron nitrate nonahydrate (0.125 mmol), zinc nitrate hexahydrate (0.25 mmol), and manganese nitrate tetrahydrate (0.125 mmol) in a mixed solvent of 20 mL methanol and 5 mL deionized water. Stir magnetically at room temperature for 10 minutes until a homogeneous yellow solution is formed. Take 0.84 g of 2-methylimidazole and dissolve it in a mixture of 20 mL of methanol and 5 mL of deionized water. After complete dissolution, mix it with the above metal salt solution and continue magnetic stirring for 30 minutes to obtain a uniform red purple precursor solution. Constant potential electrodeposition was performed using a three electrode system: pre treated NF was used as the working electrode, platinum plate as the counter electrode, and Ag/AgCl as the reference electrode. The precursor film was deposited for 800 seconds at a constant voltage of -4 V (vs. SCE). After sedimentation, the sample was washed with deionized water and vacuum dried at 60 ℃ for 6 hours. For comparative research, control group samples containing different manganese contents and without manganese doping were prepared simultaneously. According to the composition of metal elements, the experimental sample is labeled as NCFZM0.125-ZIF/NF (N: Ni, C: Co, F: Fe, Z: Zn, M: Mn).

1.2.3. Synthesis of NCFZMx-P/NF

The synthesized NCFZM0.125/NF precursor and 0.3g sodium hypophosphite monohydrate were placed in the same quartz boat. NaPO2H2 • H2O is located upstream of the tube furnace, with the precursor placed downstream. It is then pyrolyzed at 350 ℃ for 2 hours under a nitrogen atmosphere, with a temperature rise rate of 2 ℃ min-1, to obtain the sample NCFZMx-P/NF.

1.3. Electrochemical test methods

Electrodeposition and electrochemical testing were conducted on an Ivium

electrochemical workstation purchased in the Netherlands, using a three electrode system for catalytic performance testing in 1M KOH solution. Cut the prepared catalyst into 0.25 cm^{-2} and clamp it on the working electrode. Use a platinum plate as the counter electrode and Hg/HgO as the reference electrode. At the same time, use the Nernst equation to perform reversible hydrogen electrode potential energy transformation on the electrochemical test data.

$$E_{RHE} = E_{Hg/HgO} + E^{@}_{Hg/HgO} + 0.059PH \tag{1}$$

Where $E_{Hg/HgO}$ is the potential of Hg/HgO for the test with the reference electrode, $E^{@}_{Hg/HgO}$ is the standard electrode potential for the Hg/HgO reference electrode, and its value is 0.098 V; The acid-base value of the test solution is represented by pH.

The following equations are used to figure out the overpotentials:

$$\eta_{OER} = E_{RHE} - 1.23 \tag{2}$$

$$\eta_{OER} = E_{RHE} \tag{3}$$

Not all curves are compensated by the IR potential. LSV curve IR compensation is 95%.

Tafel equation:

$$\eta = a + b\lg(j) \tag{4}$$

Where η, a, b and j denote the overpotential, Tafel constant, Tafel slope and current density, respectively, the Tafel plot is obtained by plotting the logarithm of the current density lg(j) against the overpotential (η) through the polarization curve, and the Tafel slope is obtained by fitting the linear part of the Tafel plot. Given that the Tafel slope is inversely proportional to the charge transfer coefficient, it can be used as one of the indicating parameters for evaluating the electrocatalyst performance.

At a scan rate of 5 mV/s, linear scanning voltammetry (LSV) is carried out. In the frequency range from 100000 to 0.01 Hz, electrochemical impedance spectroscopy (EIS) is performed. CV can measure electrochemical double-layer capacitance (C_{dl})

within the range of -0.30 V to -0.40 V at scan rates of 20, 40, 60, 80, and 100 mV/s. The formula for calculating the electrochemically active surface area (ECSA) is as follows:

$$ECSA = C_{dl} / C_s \tag{5}$$

where Cs is the specific capacitance. Use the commonly used specific capacitance Cs, which has a value of 0.040 mF cm^{-2} in 1 M KOH.

All experiments are repeated at least three times to ensure reproducibility.

1.3 Theoretical calculation

The energy cutoff value for plane waves is set to 400 eV. All structures have been optimized based on the convergence criteria of energy of 1 × 10-5 eV and force of 0.1 eV/nm. The vacuum spacing is set to be greater than 1.5nm for surface isolation to prevent interaction between two adjacent surfaces. The computational model uses a 3 × 3 × 1 Monkhorst packaging grid for Brillouin zone sampling. Density k points (3 × 3 × 1) are used to calculate the projected density of states (PDOS).

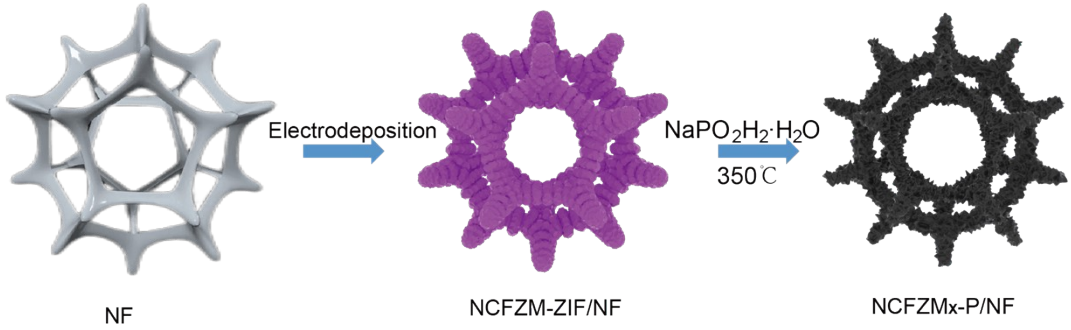

Figure S1. Flow Chart of NCFZMx-P/NF Stacked Nanosheet Synthesis on foam Nickel.

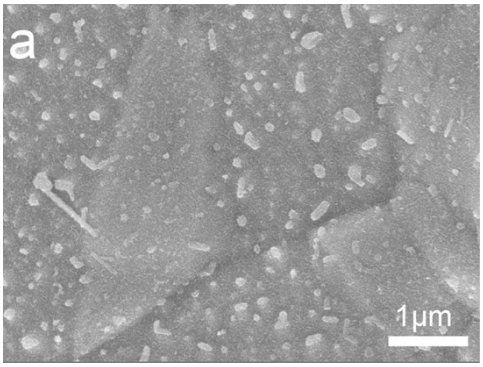

Figure S2. SEM image of NF

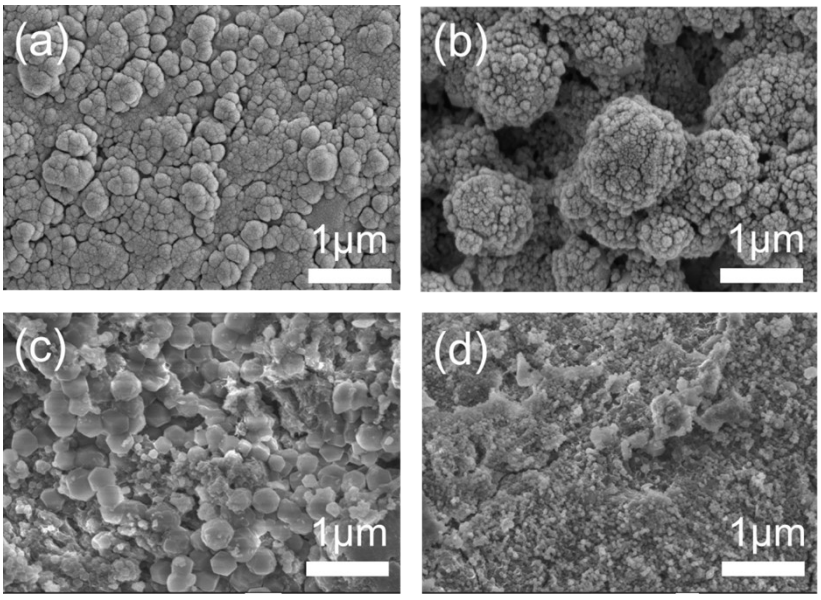

Figure S3. SEM images of (a) NCFZ-ZIF/NF, (b) $NCFZM_{0.25}$-ZIF/NF, (c) $NCFZM_{0.375}$-ZIF/NF, (d) $NCFZM_{0.5}$-ZIF/NF.

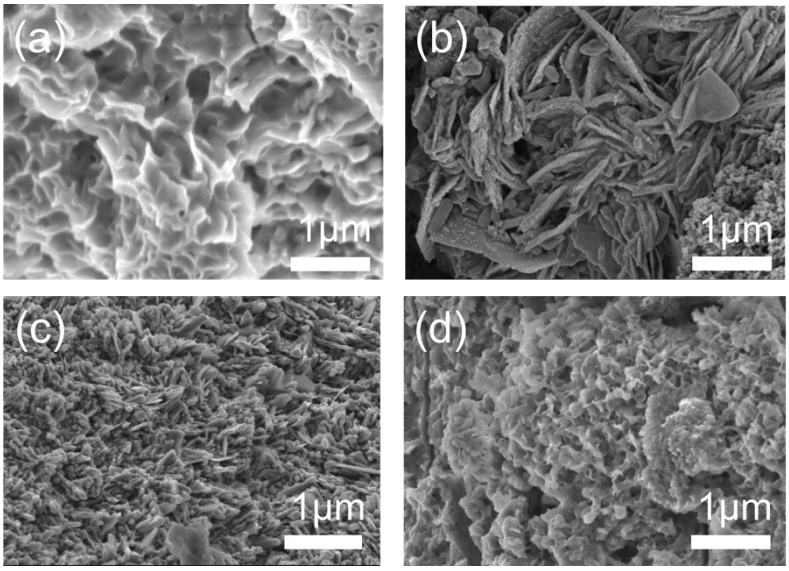

Figure S4. SEM images of (a) NCFZP/NF, (b) NCFZM$_{0.25}$P/NF, (c) NCFZM$_{0.375}$P/NF, (d) NCFZM$_{0.5}$P/NF.

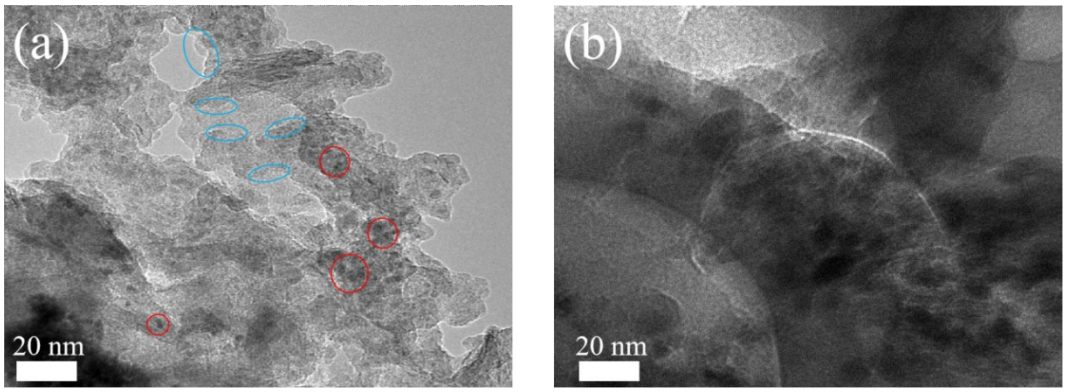

Figure S5. (a) TEM image of NCFZM$_{0.125}$P/NF (b) TEM image of NCFZM$_{0.125}$P/NF.

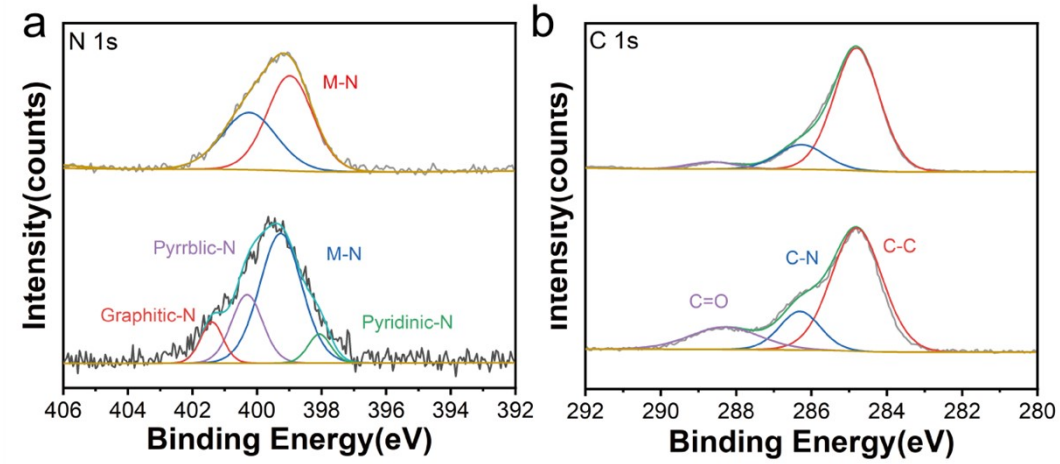

Figure S6. High resolution XPS spectra of (a) N 1s (b) C 1s for NCFZM$_{0.125}$-ZIF/NF and NCFZM$_{0.125}$P/NF.

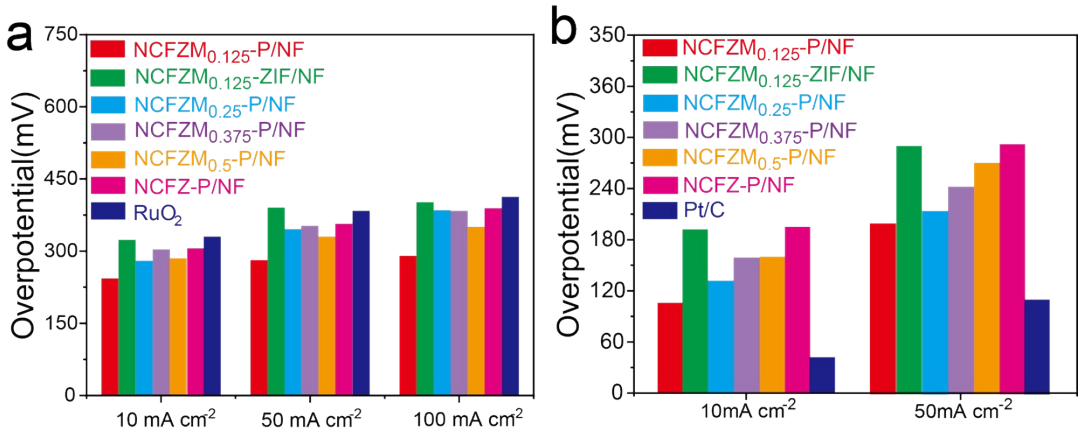

Figure S7. OER and HER Overpotential Histogram

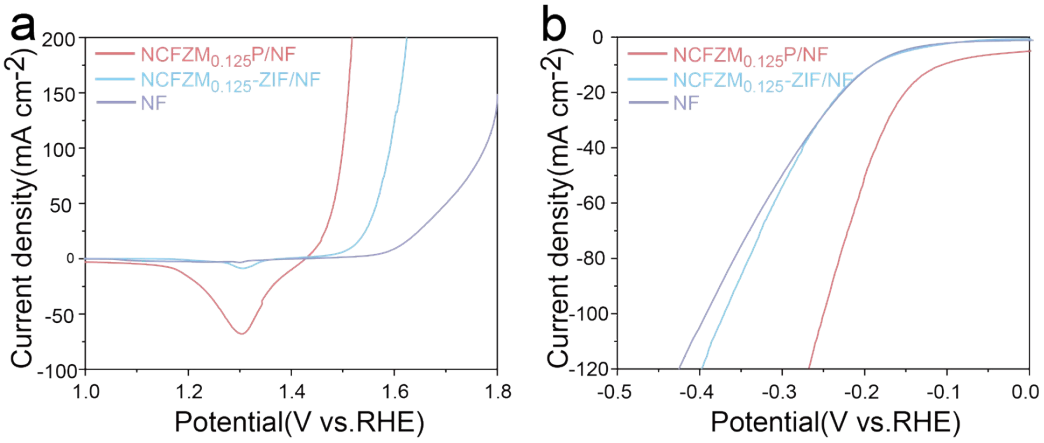

Figure S8. Comparison chart with LSV of NF

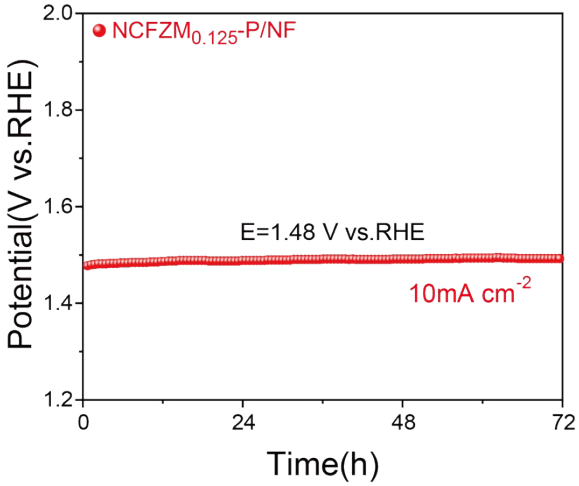

Figure S9. Constant current OER curve of $NCFZM_{0.125}$-P/NF in 1.0 M KOH solution for 72 hours

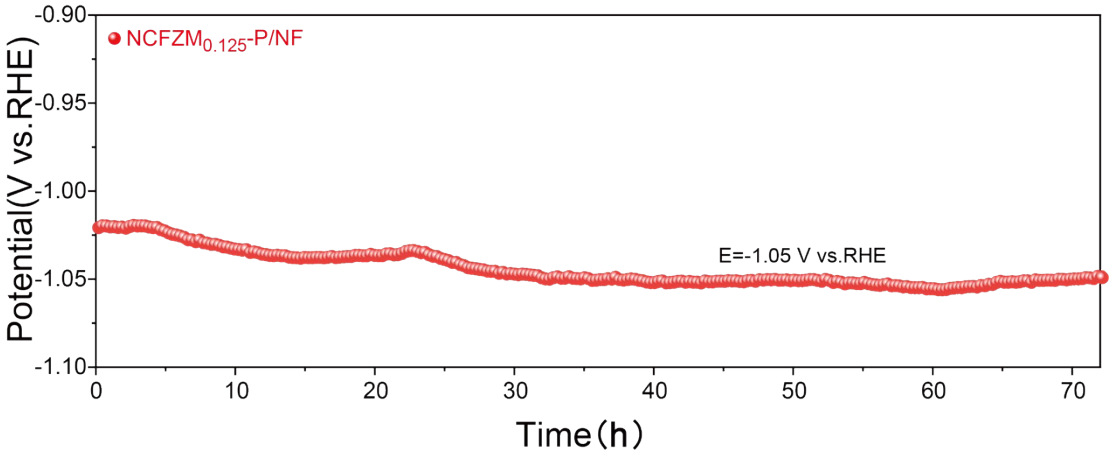

Figure S10. Constant current HER curve of $NCFZM_{0.125}$-P/NF in 1.0 M KOH solution for 72 hours

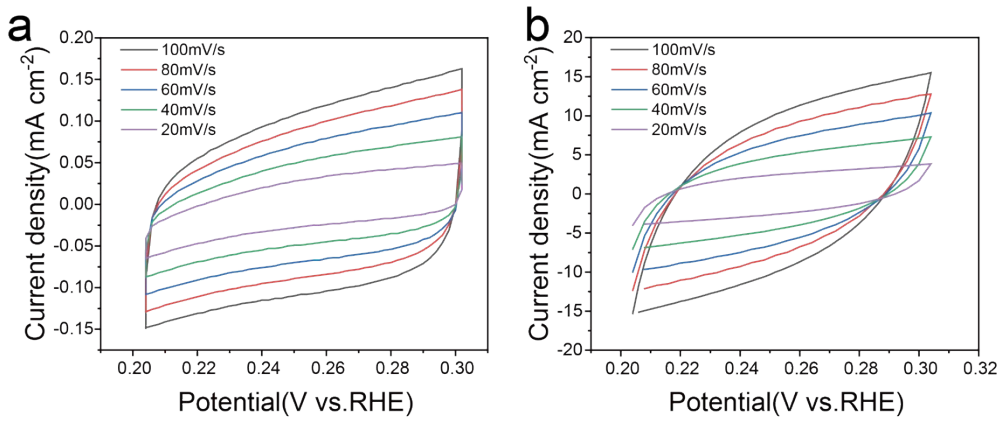

Figure S11. CV curves of (a) $NCFZM_{0.125}$-ZIF/NF and (b) $NCFZM_{0.125}$P/NF.

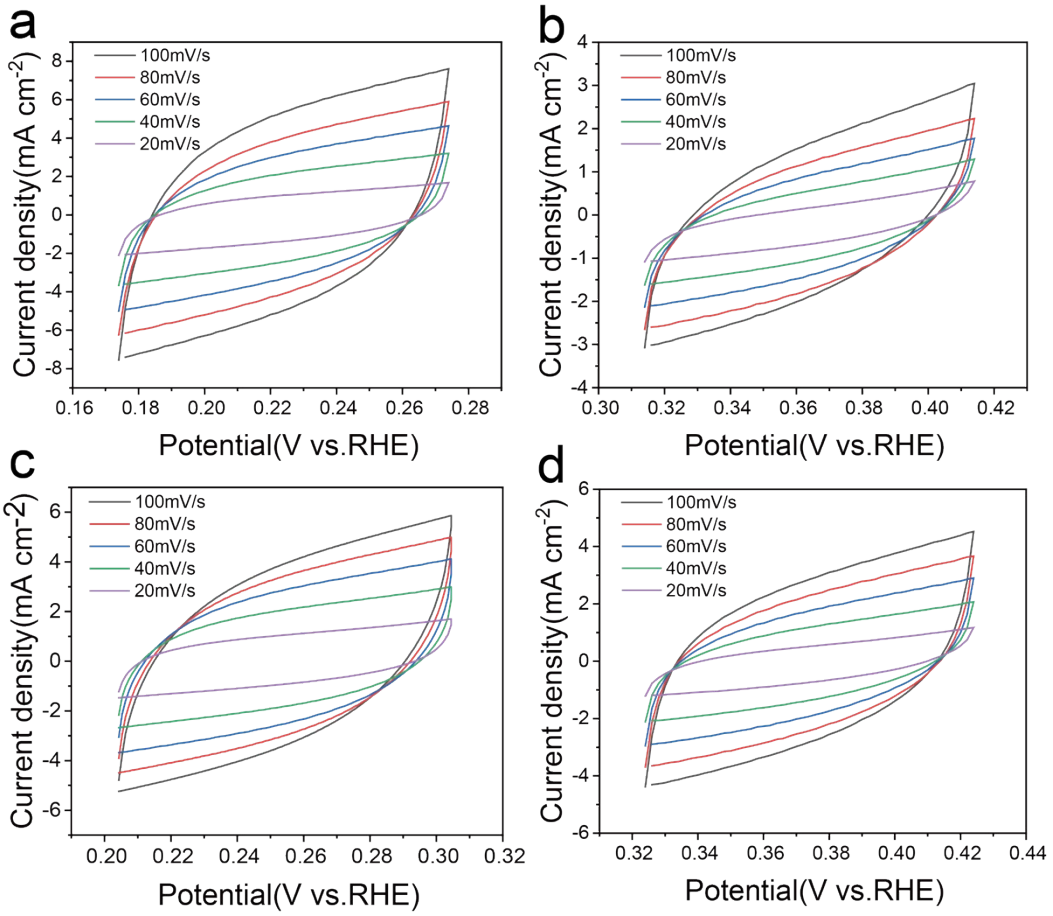

Figure S12. CV curves of (a) NCFZP/NF , (b) NCFZM$_{0.25}$P/NF, (c) NCFZM$_{0.375}$P/NF and (d) NCFZM$_{0.5}$P/NF.

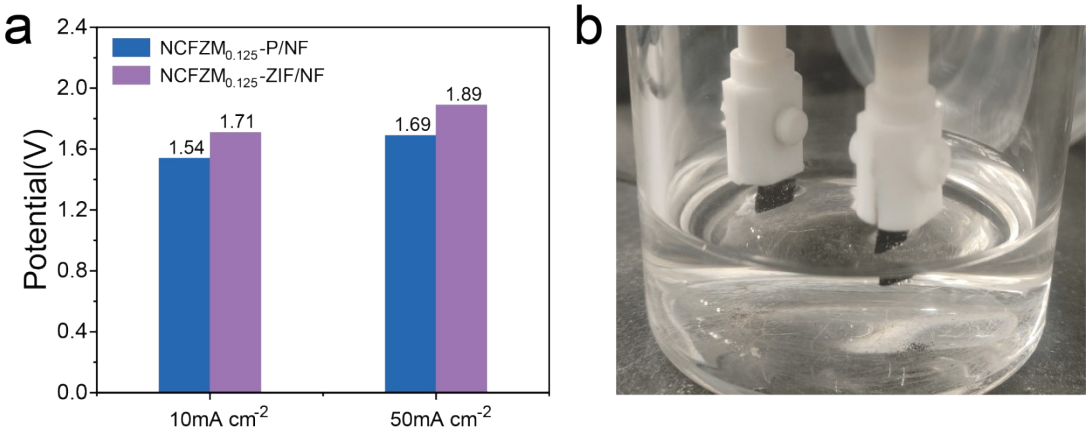

Figure S13. (a) Overpotentials of NCFZM$_{0.125}$-P/NF and NCFZM-ZIF$_{0.125}$/NF at different current densities. (b) Schematic diagram of alkaline electrolysis cell

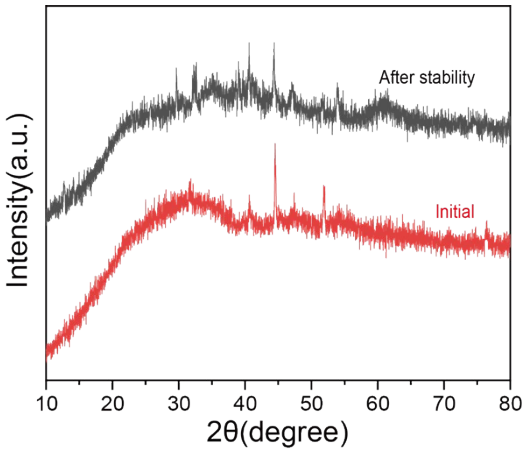

Figure S14. XRD image of $NCFZM_{0.125}$-P/NF after stability test

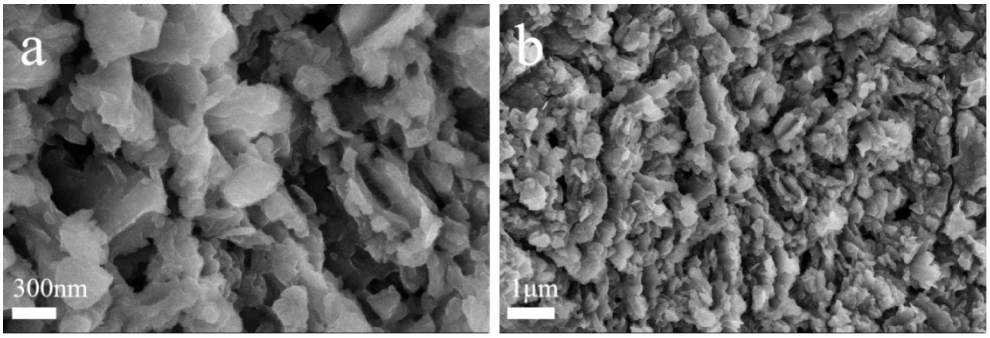

Figure S15. SEM image of (a,b) $NCFZM_{0.125}P$/NF after stability test.

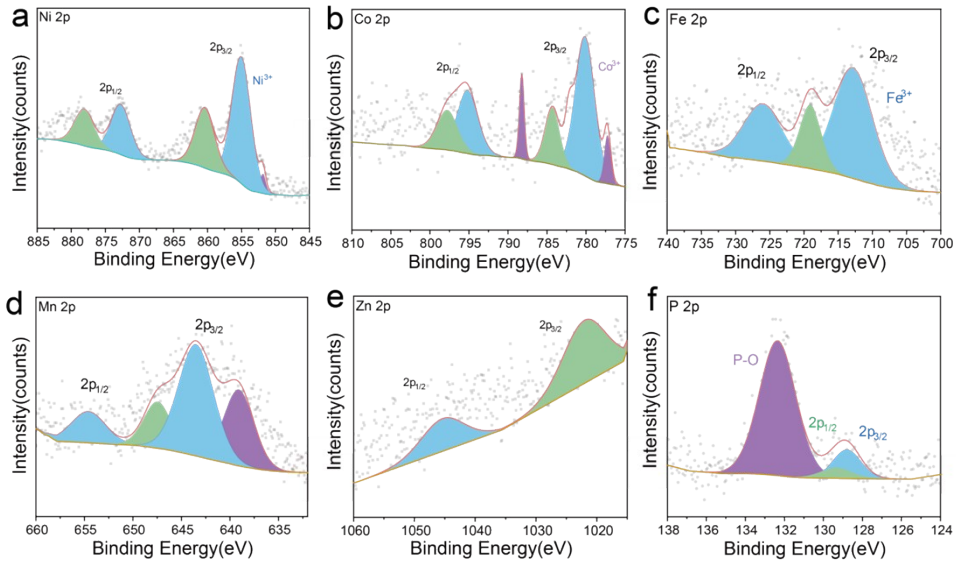

Figure S16. High resolution XPS spectra of (a) Ni 2p (b) Co 2p (c) Fe 2p (d) Mn 3d (e) Zn 2p (f) P 2p for $NCFZM_{0.125}P$/NF after stability test.

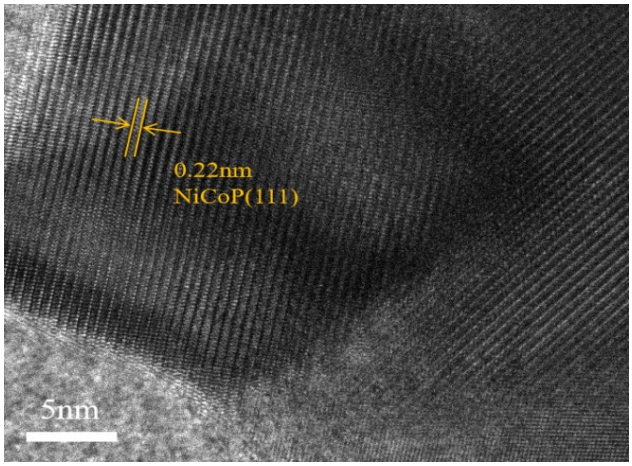

Figure S17. TEM image of NCFZM$_{0.125}$P/NF after stability test

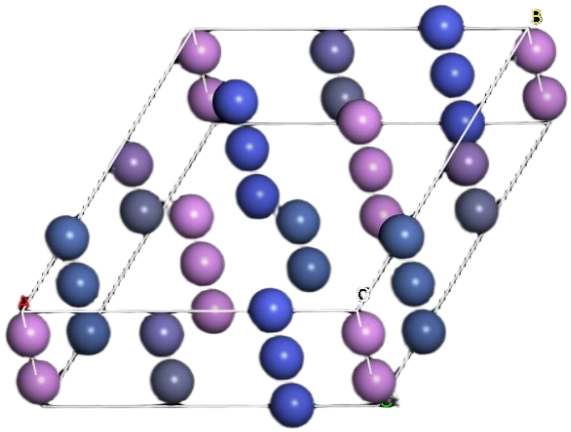

Figure S18. Theoretical structural model of NFCZM$_{0.125}$P/NF

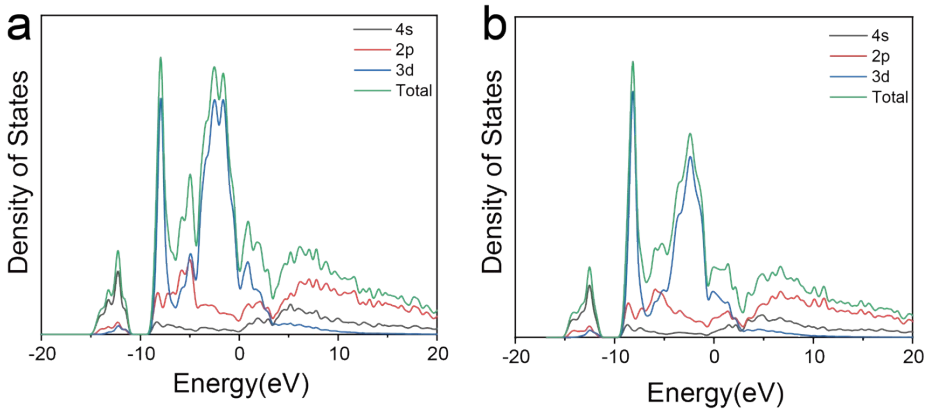

Figure S19. Plot of total density of states and different orbital density of states for NCFZ-P/NF

Table S1. ICP-OES results (wt% and at%) of as-deposited ZIF and phosphorized sample

Element	As-deposited ZIF (wt%)	Phosphorized (wt%)	As-deposited ZIF (at%)	Phosphorized (at%)
Ni	95.195	85.152	91.64	76.83
Co	0.461	0.733	0.44	0.66
Fe	0.072	0.138	0.07	0.13
Mn	0.261	0.529	0.27	0.51
Zn	0.989	0.822	0.85	0.67
P	/	8.066	/	13.8

Table S2. Reproducibility of the "0.125" sample (three batches, normalized at% of Co, Fe, Mn, Zn)

Batch	Ni (wt%)	Co (wt%)	Fe (wt%)	Mn (wt%)	Zn (wt%)
1	95.195	0.461	0.072	0.261	0.989
2	95.01	0.472	0.071	0.255	0.976
3	95.13	0.468	0.073	0.258	0.982
RSD	0.10%	1.21%	1.40%	1.16%	0.66%

Note: RSD stands for Relative Standard Deviation, which is used to measure the consistency of data across three independent composite samples; a lower value indicates better reproducibility.

Table S3. XPS fitting data for $NCFZM_{0.125}$-ZIF/NF

Element	Peak	B.E. (eV)	Chemical state	FWHM (eV)	Rel. area (%)	Background
Ni 2p	$2p_{3/2}$	855.18eV	Ni^{2+}	2.79	38.5%	
	Satellite	861.23eV	Ni^{2+}	5.3	26.30%	
	$2p_{1/2}$	872.8eV	Ni^{2+}	2.79	18.50%	
	Satellite	879.26eV	Ni^{2+}	5.3	16.70%	
Co 2p	$2p_{3/2}$	780.75eV	Co^{2+}	2.99	49.89%	
	Satellite	785.76eV	Co^{2+}	3.5	16.11%	
	$2p_{1/2}$	796.37eV	Co^{2+}	2.99	25.72%	
	Satellite	801.97eV	Co^{2+}	3.5	8.28%	
Fe 2p	$2p_{3/2}$	711.51	Fe^{3+}	7.37	51.96%	Smart
	$2p_{1/2}$	716.75	Fe^{3+}	7.38	25.21%	
	Satellite	722.99	Fe^{3+}	5	22.83%	
Mn 2p	$2p_{3/2}$	641.12	Mn^{2+}	7.62	41.70%	
	Satellite	652.6	Mn^{2+}	7.62	22.70%	
	$2p_{1/2}$	645	Mn^{2+}	5.2	18.10%	
	Satellite	656.625	Mn^{2+}	5.2	16.50%	
Zn 2p	$2p_{3/2}$	1021.59	Zn^{2+}	2.4	65.86%	
	$2p_{1/2}$	1044.65	Zn^{2+}	2.4	34.14%	

Table S4. XPS fitting data for $NCFZM_{0.125}$-P/NF

Element	Peak	B.E. (eV)	Chemical state	FWHM (eV)	Rel. area (%)	Background
Ni 2p	$2p_{3/2}$	852.26	Ni-P	1.94	31.50%	Smart
	$2p_{3/2}$	855.5	Ni^{2+}	2.05	20.19%	
	Satellite	859.67	Ni^{2+}	3.6	14.13%	
	$2p_{1/2}$	868.24	Ni-P	1.97	11.72%	
	$2p_{1/2}$	872.69	Ni^{2+}	2.05	9.87%	
	Satellite	876.73	Ni^{2+}	3.55	12.59%	
Co 2p	$2p_{3/2}$	777.82	Co-P	1.57	40.29%	
	$2p_{3/2}$	780.55	Co^{2+}	3.43	21.30%	
	Satellite	784.02	Co^{2+}	2.4	4.60%	
	$2p_{1/2}$	792.83	Co-P	1.87	14.59%	
	$2p_{1/2}$	796.6	Co^{2+}	3.03	11.47%	
	Satellite	800.5	Co^{2+}	2.54	7.74%	
Fe 2p	$2p_{3/2}$	710.58	Fe^{3+}	4.79	20.14%	
	Satellite	714.59	Fe^{3+}	5	38.53%	
	$2p_{3/2}$	719.19	Fe^{3+}	3.5	19.49%	
	$2p_{1/2}$	724.53	Fe^{3+}	4.79	8.84%	
	Satellite	727.54	Fe^{3+}	5	7.02%	
	$2p_{1/2}$	731.68	Fe^{3+}	3.5	5.98%	
Mn 2p	$2p_{3/2}$	641.48	Mn^{2+}	2.97	45.55%	
	$2p_{3/2}$	643.19	Mn^{4+}	2.72	14.94%	
	Satellite	646.17	Mn^{2+}	2.69	16.32%	
	$2p_{1/2}$	652.94	Mn^{2+}	2.97	7.28%	
	$2p_{1/2}$	654.54	Mn^{4+}	2.72	7.67%	
	Satellite	657.37	Mn^{2+}	2.68	8.24%	
Zn 2p	$2p_{3/2}$	1021.44	2+	1.94	62.55%	
	$2p_{1/2}$	1044.27	2+	2.04	37.45%	
P 2p	$2p_{3/2}$	129.39	M-P	1.5	66.98%	
	Satellite	128.46	M-P	0.9	24.57%	
	$2p_{1/2}$	132.80	P-O	1.5	16.57%	

Table S5. Comparison of the OER activity of the NCFZMP/NF with other electrocatalysts in basic condition.

Catalysts	Electrolyte	Overpotential (mV, @ 10 mA cm^{-2})	Tafel slope (mV dec-1)	Reference
$NCFZM_{0.125}P$/NF	**1.0 M KOH**	**218**	**57.57**	**This work**
CoP/Ni_2P/Fe_2P	1.0 M KOH	260	66.5	1
Ni_1Co_1–P	1.0 M KOH	343	77	2
FeNi/Ni_2P@NC	1.0 M KOH	323	60.3	3
Ni_2P/rGO	1.0 M KOH	221	105.7	4
A-Ni_2P/Cu_3P	1.0 M KOH	262	78.3	5
Fe-NiO/Ni_2P	1.0 M KOH	242	49.1	6
Co_2P@N-C-900	1.0 M KOH	352	84.6	7
Co_2P/WO_{3-x}/CC	1.0 M KOH	254	58.32	8
Co_2P/NPC	1.0 M KOH	320	59.6	9
Co_2P-1/Ni_2P-1 @NF	1.0 M KOH	310	69.9	10

Table S6. Comparison of the HER activity of the NCFZMP/NF with other electrocatalysts in basic condition.

Catalysts	Electrolyte	Overpotential (mV, @ J mA cm^{-2})	Tafel slope (mV dec^{-1})	Reference
$NCFZM_{0.125}P/NF$	**1.0 M KOH**	**106**	**119.45**	**This work**
Fe_2P-Ni_2P/Co_2P	1.0 M KOH	125	60.3	11
Co_2P/CoP/NC	1.0 M KOH	184	82	12
Ni_1Co_1–P	1.0 M KOH	169	68	2
CP-350	1.0 M KOH	181	112	13
NiMoO-SP/Ti	1.0 M KOH	159	77	14
Fe-NiO/Ni_2P	1.0 M KOH	141	111	6
Zr-MOF/Ni_2P@NF-250	1.0 M KOH	143	40.49	15

Table S7. Comparison of the full water-splitting performances of NCFZMP/NF with other other electrocatalysts in 1 M KOH at the current density of 10 and 50 mA cm^{-2}.

Catalysts	**Cell voltages (V) @ J (mA cm^{-2})**	**Reference**
$NCFZM_{0.125}P$/NF	1.53@10 mA cm^{-2} 1.69@10 mA cm^{-2}	**This work**
CoNiP/MP Ni	1.78@10 mA cm^{-2}	16
HOF-$Co_{0.5}Fe_{0.5}$/NF	1.66@10 mA cm^{-2}	17
Co_2P/CoNPC	1.63@10 mA cm^{-2}	18
Co-BTC MOF	1.64@10 mA cm^{-2}	19
CoNiP/NF	2.03@10 mA cm^{-2}	20
CoP/GO-400	1.62@10 mA cm^{-2}	21
Ni/Mo_2C-PC	1.7@10 mA cm^{-2}	22
NiSe/NF	1.66@10 mA cm^{-2}	23
Ni_3S_2/NF	1.63@10 mA cm^{-2}	24
Ni_2Fe@NC	1.7@10 mA cm^{-2}	25

Table S8. Comparison of Valence States and Coordination in OER and HER Before and After the Reaction

Element	Peak assignment	Fresh	After HER	After OER
Ni 2p	Ni–P	852.26	Weaker	Disappeared
	Ni^{2+}	855.5	855.6	855.8
Co 2p	Co–P	777.82	777.7 (	Weaker
	Co^{2+}	780.55	780.6	780.8
Fe 2p	Fe–P	/	/	/
	Fe^{3+}	710.58	710.6	710.7
Mn 2p	Mn^{2+}	641.48	641.5	Weaker
	Mn4+	643.19	643.2	Stronger
P 2p	M–P	129.39	Weaker	Weaker
	P–O	132.80	Stronger	Stronger
Zn 2p	Zn^{2+}	1021.44	1021.4	1021.4

References

1. C. Zhang, Z. Xing, Y. Peng, H. Zhou, L. Zhang and Z.-H. Lu, *Fuel*, 2024, 365.
2. C. Shuai, Z. Mo, X. Niu, P. Zhao, Q. Dong, Y. Chen, N. Liu and R. Guo, *J. Alloy. Compd.*, 2020, 847.
3. T. Yu, Y. Zhang, J. Zhou, M. Feng, Z. Zhang and Y. Zhou, *J. Mater. Sci.*, 2024, 59, 21710–21720.
4. S. Luo, R. Wang, P. Hei, L. Gao, J. Yang and T. Jiao, *Colloids Surf. A Physicochem. Eng. Asp.*, 2021, 612.
5. J. Lin, Y. Yan, T. Xu, J. Cao, X. Zheng, J. Feng and J. Qi, *J Colloid Interface Sci*, 2020, 564, 37–42.
6. L. Xu, L. Zheng, Y. Xu, C. Hao, X. Hu and Y. Wang, *J Colloid Interface Sci*, 2025, 679, 109–118.
7. K. Wang, R. Zhang, Y. Guo, Y. Liu, Y. Tian, X. Wang, P. Wang and Z. Liu, *Energies*, 2023, 16.
8. H. Guo, L. Pan, H. Jiang, M. Gao, H. Wang, A. Khan, N. A. Siddiqui and J. Lin, *Chemistry*, 2025, 31, e202402907.
9. D. Zhang, P. Sun, Z. Zuo, T. Gong, N. Huang, X. Lv, Y. Sun and X. Sun, *J. Electroanal. Chem.*, 2020, 871.
10. H. Zhao, J. Liang and Y. Zhao, *J. Alloy. Compd.*, 2022, 907.
11. W. Chen, S. Chen, M. Guo, X. Jiang, J. Xia, M. Chen, Y. Xiong and X. Qian, *Int. J. Hydrog. Energy*, 2024, 78, 851–860.
12. Y. Lei, F. Lin, N. Hong, J. Zhang, Y. Wang, H. Ben, J. Li, L. Ding and L. Lv, *Materials (Basel)*, 2023, 17.
13. S. Kumaravel, T. Joseph Sahaya Anand, P. Saravanan, Y. Haldorai and R. T. R. Kumar, *Chem. Select*, 2024, 9.
14. Y. Wang, T. Williams, T. Gengenbach, B. Kong, D. Zhao, H. Wang and C. Selomulya, *Nanoscale*, 2017, 9, 17349–17356.
15. Y. Li, N. He, X. Chen, B. Fang, X. Liu, H. Li, Z. Gong, T. Lu and L. Pan, *J Colloid Interface Sci*, 2024, 656, 289–296.

16. Z. Xu, S. Li, W. Lu, X. Dou, Y. Wu, J. Zeng, Y. Dou, J. Zhang, J. Wei and L. Yu, *Fuel*, 2023, 348.
17. F. Q. Liu, J. W. Liu, Z. Gao, L. Wang, X.-Z. Fu, L. X. Yang, Y. Tao, W. H. Yin and F. Luo, *App. Catal. B: Environ.*, 2019, 258.
18. H. Liu, J. Guan, S. Yang, Y. Yu, R. Shao, Z. Zhang, M. Dou, F. Wang and Q. Xu, *Adv. Mater.*, 2020, 32, e2003649.
19. S. Naik Shreyanka, J. Theerthagiri, S. J. Lee, Y. Yu and M. Y. Choi, *Chem. Eng. J.*, 2022, 446.
20. H. Liu, R. Huang, W. Chen, Y. Zhang, M. Wang, Y. Hu, Y. Zhou and Y. Song, *Appl. Surf. Sci.*, 2021, 569.
21. L. Jiao, Y. X. Zhou and H. L. Jiang, *Chem Sci*, 2016, 7, 1690–1695.
22. Z. Y. Yu, Y. Duan, M. R. Gao, C. C. Lang, Y. R. Zheng and S. H. Yu, *Chem Sci*, 2017, 8, 968–973.
23. C. Tang, N. Cheng, Z. Pu, W. Xing and X. Sun, *Angew. Chem. Int. Ed.*, 2015, 54, 9351–9355.
24. L. L. Feng, G. Yu, Y. Wu, G. D. Li, H. Li, Y. Sun, T. Asefa, W. Chen and X. Zou, *J Am Chem Soc*, 2015, 137, 14023–14026.
25. J. Chang, S. Zang, J. Li, D. Wu, Z. Lian, F. Xu, K. Jiang and Z. Gao, *Electrochim. Acta*, 2021, 389.